A&A 468, 1063–1073 (2007)
DOI: 10.1051/0004-6361:20066060

Astronomy & Astrophysics

Fourier method of determining the rotational velocities in OB stars⋆,⋆⋆

S. Simón-Díaz[1,2] and A. Herrero[1,3]

[1] Instituto de Astrofísica de Canarias, 38200 La Laguna, Tenerife, Spain
e-mail: sergio.simon-diaz@obspm.fr
[2] LUTh, Observatoire de Meudon, 92195 Meudon Cedex, France
[3] Departamento de Astrofísica, Universidad de La Laguna, 38071 La Laguna, Spain

Received 18 July 2006 / Accepted 6 March 2007

ABSTRACT

Aims. We present a comprehensive study that applies the Fourier transform to a sample of O and early B-type stars (either dwarfs, giants, or supergiants) to determine their projected rotational velocities. We then compare them with previous values obtained with other methods and seek evidence of extra broadening in the spectral lines

Methods. The Fourier technique, extensively used in the study of cooler stars, has only been marginally applied to early-type stars. The comparison of $v \sin i$ values obtained through the FT and FWHM methods shows that the FWHM technique must be used with care in the analysis of OB giants and supergiants and when it is applied to He I lines. In contrast, the FT method appears to be a powerful tool for deriving reliable projected rotational velocities and separating the effect of rotation from other broadening mechanisms present in these stars.

Results. The analysis of the sample of OB stars shows that while dwarfs and giants display a broad range of projected rotational velocities, from less than 30 up to 450 km s^{-1}, supergiants have in general values close to or below 100 km s^{-1}. The analysis has also definitely shown that, while the effect of extra broadening is negligible in OB dwarfs, it is clearly present in supergiants. When examining the behavior of the projected rotational velocities with the stellar parameters and across the HR diagram, we conclude, in agreement with previous researchers, that the rotational velocity should decrease when the stars evolve. On the contrary, macroturbulence may be constant, therefore resulting in an increasing importance as compared to rotation when the stars evolve.

Key words. stars: early-type – stars: rotation – techniques: spectroscopic – methods: data analysis

1. Introduction

Together with mass and metallicity, stellar rotation (i.e. stellar angular momentum) determines the formation, structure, and evolution of a star. Moreover, it is a necessary property for a large number of important processes, like the solar dynamo or stellar activity. In the realm of massive stars, rotation is becoming increasingly important. It is thought to be the reason for internal mixing mechanisms that would bring CNO-processed material and transport inner angular momentum to the stellar surface (Maeder & Meynet 2000). Coupled with stellar winds, it can strongly alter the evolution of the star and the theoretical Eddington limit. Equally important, the coupling with stellar winds imposes a dependence of the rotational velocity itself on metallicity during the evolution of high-mass stars (Maeder & Meynet 2001). Consequently, massive stars in the Magellanic Clouds are expected to have higher rotational velocities on average, and more CNO contamination in their atmospheres.

Since present evolutionary stellar models take this rotational velocity into account and consider it as an important parameter in the stellar evolution, accurate determination of stellar rotational velocities in massive stars is required, not only to constrain these stellar evolutionary models, but also to understand the physics of massive stars and their dependence on metallicity.

Several methods for determining of projected rotational velocity ($v \sin i$) in isolated early-type stars can be found in the literature. The most commonly used ones are

1. The full-width-half-maximum (FWHM) of the observed line profile is measured and related to the $v \sin i$ (FWHM method).
2. The observed spectrum is cross-correlated against a *template* spectrum with a low rotational velocity. The Gaussian width of the cross-correlation function is directly related to the projected rotational velocity of the star if rotation is the dominant broadening mechanism of the photospheric lines.
3. The observed line profiles are compared with synthetic ones calculated from model atmospheres that are convolved with the corresponding broadening functions. Although this is a very accurate method if the broadening functions are well-known, too much computational time is required. Reducing that time (e.g., using model grids) also reduces the accuracy.
4. The Fourier transform of the line profile is calculated. The position of zeroes present in this Fourier transform depends on the $v \sin i$.

Being very fast and easy to use, the FWHM method has been extensively applied to measuring the projected rotational velocities in OB stars (viz. Slettebak 1975; Herrero et al. 1992; Abt et al. 2002; Strom et al. 2005). The cross-correlation

⋆ The INT and WHT telescopes are operated on the island of La Palma by the RGO in the Spanish Observatorium of El Roque de los Muchachos of the Instituto de Astrofísica de Canarias.

⋆⋆ Tables 2–10 are only available in electronic form at http://www.aanda.org

method was applied by Penny (1996), Howarth et al. (1997) and Penny et al. (2004) to IUE and STIS spectra of O-type stars and early B-type supergiants. The studies coming from both methodologies (i.e., FWHM and cross-correlation) allow us to have $v \sin i$ measurements of large samples of OB stars with different luminosity classes; however, the main limitation of these techniques is that they do not allow for the separation of rotational broadening from other possible, extra broadening mechanisms, usually referred to as macroturbulence (although the actual physical mechanism – or mechanisms – remains unknown). In fact, this is a delicate and quite important task, since many works find an absence of narrow-lined OB stars. This result is supposedly an indirect proof of a non-negligible line broadening mechanism in addition to rotation in these stellar objects, especially in the case of giants and supergiants (viz. Slettebak 1956; Conti & Ebbets 1977; Howarth et al. 1997).

The fitting to broadened synthetic profiles makes it possible to distinguish between different broadening mechanisms and also to determine other stellar parameters, but as discussed before, a large effort is required to use it accurately. Furthermore, quite good quality spectra (i.e. high signal-to-noise ratio, *SNR*, and spectral resolution) are required to disentangle the various broadening mechanisms that may affect the line profiles, and the derived values may depend on the considered models and the definition of the broadening functions. An early attempt to separate the rotational and macroturbulent contributions to the line broadening in O- and early B-type stars was performed by Slettebak (1956), however he found that the quality of his spectra was not good enough to get any conclusive solution.

More recently, Ryans et al. (2002) analyzed the high-quality spectra of twelve B-type supergiants. They compared observed and synthetically broadened lines using a χ^2 technique and find for their survey of B-type supergiants that, while models dominated by rotation provide unsatisfactory fits, those where macroturbulence dominates and rotation is negligible (as a broadening agent) were acceptable.

Even though it is also very fast and easy to use, the Fourier method, a technique pioneered using cool stars, has been only marginally applied in the study of OB stars. This technique allows the $v \sin i$ to be easily derived independently of any other broadening mechanism affecting the line profile. There are numerous papers illustrating its use in determining $v \sin i$ in later type stars (Smith 1976; Gray 1980; Royer et al. 2002a,b; Reiners & Schmitt 2003); however, there is no comprehensive study applying this technique to early-type stars except the one by Ebbets (1979), who analyzed a sample of 16 objects, but the limited quality of the spectra allowed him to obtain estimations of the macroturbulence for only half the objects in the sample. Recently, Simón-Díaz et al. (2006) have applied the Fourier method to a small sample of OB stars in the Orion nebula. The strength of this method was shown in the study of the main ionizing star of this nebula, an O7 V star with a well-known rotational period of ∼15 days, which conflicts with the $v \sin i$ derived from the FWHM method, but agrees with the Fourier technique.

Following the ideas of the present paper and Ryans et al. (2002), Dufton et al. (2006a) have recently analyzed the high-resolution spectra for 24 SMC and Galactic B-type supergiants to estimate the contributions of both macroturbulence and rotation to the broadening of their metal lines. See also the analysis of periodically variable B supergiants by Lefever et al. (2006).

This paper has three main objectives. First, we extend the work presented in Simón-Díaz et al. (2006) illustrating the strength of the Fourier method in the analysis of early type stars. Second, we provide new, more accurate values for the rotational velocities of OB stars and estimate the role played by other broadening mechanisms; and third, we extend the work by Dufton et al. (2006a) and Lefever et al. (2006) towards early spectral types.

From our archive we restored the spectra of several OB stars, obtained in different observing campaigns, for a comprehensive determination of the rotational velocities through the Fourier analysis method. But first, a formal study was made to determine the range of applicability of this methodology to OB stars.

The paper is structured in four main parts as follows, beginning with a short review of the Fourier methodology, as well as some formal tests for the case of massive stars in Sect. 2. The determination of the projected rotational velocities of the sample of OB type stars is presented in Sect. 3. Finally, the discussion and the main conclusions are presented in Sects. 4 and 5.

2. Testing the Fourier method in early-type stars

The theoretical basis of this methodology was well-established by Gray (1976; see also the latest edition of the book, published in 2005). Here, we briefly summarize the main characteristics of the method, as needed to understand its advantages and limitations and to evaluate the results presented in Sect. 3. We also present examples specifically aimed at its application to early-type stars. For a more precise description of the methodology and its applications to late-type stars, we refer to Gray's book (see above for references). Additional details may be found in the pioneering articles by Gray (1973, 1975), Smith (1976), and Smith & Gray (1976). Some objections to its validity in special cases can be found in Mihalas (1979) and Bruning (1984).

In a simple way, an observed stellar line profile may be considered to consist of the convolution of an intrinsic profile with the rotational, macroturbulent, and instrumental profiles. The intrinsic profile includes natural and thermal broadenings, as well as other contributions, such as those due to microturbulence and Stark effect. The Fourier method (FT) of determining $v \sin i$ (cf. Gray 1976) is based on the fact that, between the previous broadening profiles, only the rotational function is expected to have zeroes in its Fourier transform (except for high values of microturbulence; see below). As first described by Carroll (1933), the position of these zeroes in frequency space depends on the $v \sin i$ of the star, so that the frequency of the first zero (σ_1) is related to the rotational velocity through

$$\frac{\lambda}{c} v \sin i \, \sigma_1 = 0.660. \quad (1)$$

Since convolutions transform into products in Fourier space, these zeroes will also appear in the total transform function of the line profile. Therefore, it is in principle possible to determine, independently of any other broadening mechanism, the $v \sin i$ of a star once the position of the first of those zeroes is identified in the Fourier transform of the line profile[1].

Other mechanisms may contribute zeroes to the total Fourier transform, depending on their profiles in the wavelength domain. Note, for example, that microturbulence can also add zeroes, when strong lines are considered, due to the boxiness caused by it in saturated lines (Gray 1976). However, those zeroes arising from saturation in the Fourier space appear at higher frequencies than those for rotation, so there is rarely any confusion between them, except for those cases with low $v \sin i$.

[1] This argument is only valid under the hypothesis considered by the convolution method, which assumes that the effects of the different broadening mechanisms act independently to broaden the emergent flux profile (Mihalas 1979).

2.1. Some formal tests for massive stars

The properties and advantages of the Fourier method, particularly in distinguishing among physical processes that produce very similar profiles in the wavelength domain, have already been discussed and illustrated in the works mentioned above. Here we present a few applications to the particular case of early-type stars.

For this formal test we used FASTWIND (Santolaya-Rey et al. 1997; Puls et al. 2005) theoretical profiles from a model with $T_{\rm eff} = 30\,000$ K, $\log g = 4.0$ (an early B dwarf) and convolved with different broadening profiles. Thermal and microturbulence broadenings were included in the line calculation in the usual way.

For the rotational broadenings we considered the usual formulation adopted for the rotational broadening (Gray 1976), which assumes a rotational profile that is convolved with the flux profile. As shown by Conti and Ebbets (1977), this approximation may produce a small overestimation of the derived rotational velocity of fast rotators. However, as shown by these authors, the effect is negligible below 200 km s^{-1} and remains weak above that value.

The treatment of macroturbulence is a more delicate issue. Several authors have pointed out indirect evidence of some type of macroturbulent broadening acting in the case of OB stars (viz. Slettebak 1956; Conti & Ebbets 1977; Howarth et al. 1997); however, its behavior is still not understood well. To a first order, we consider an isotropic macroturbulence described by a Gaussian distribution of velocities. Some notes on other possible descriptions of the macroturbulent broadening are given in Sect. 4.

Finally, in some cases, noise was added to the synthetic spectra by using a Poissonian distribution of noise generated with RANDOMN in IDL.

A first test was performed to study how well this method works when different lines from various elements present in the stellar spectrum of OB stars are considered. Our main purpose here is to see whether the Stark broadening affects the use of H and He lines as $v \sin i$ indicators. This is particularly important when comparing metal and He lines, as the latter have sometimes been proposed for $v \sin i$ measurements in early type stars using the FWHM method, particularly when the metal lines were faint and shallow, either because of the very early spectral type or the high rotational velocity.

To graphically compare results from different lines, a $\sigma\lambda$ baseline was used, as the position of the first zero associated with the $v \sin i$ depends on λ (this is equivalent to a $1/v$ scale, see Eq. (1)). Figure 1 shows the result of this study. The Fourier technique was applied to several FASTWIND synthetic lines from different elements. As can be seen, the agreement between the various lines is excellent (even when the lines He I λ4387 or H$_\beta$ are used), which indicates that even the strongly Stark broadened Balmer lines can be used with the Fourier method, in principle, as $v \sin i$ diagnostics. Note that the power of the Fourier transform of the He I and H lines concentrates at low frequencies, diminishing more rapidly than for the other lines when higher frequencies are considered. This is an effect produced by the presence of non-rotational broadening mechanisms affecting the line profile (i.e. Stark broadening). As in the case of lines affected by macroturbulence, it will have consequences in noisy spectra.

How are these results affected by the noise present in real spectra? As mentioned by Smith & Gray (1976), random noise produces a "white noise" in Fourier space (i.e. statistically constant with Fourier frequency). Therefore at higher frequencies, where the power of the signal transform drops, the "white noise" dominates and hides the characteristics of the signal transform. This effect is illustrated in Fig. 2. A strong synthetic O II line was convolved with two sets of rotational and macroturbulent broadenings: ($v \sin i$, $v_{\rm m}$) = (50, 0) and (50, 50) km s^{-1}. Additionally, a Poissonian distribution of noise, corresponding to an $SNR = 200$, was added to both synthetic lines. Figure 2 compares the Fourier transforms corresponding to the pure and noisy synthetic profiles. For these cases, the white noise level is located at $\sim 10^{-2}$. When the profile is only affected by a rotational broadening, the signal corresponding to the first zero is far above the noise level. This first zero can be perfectly identified, and hence the $v \sin i$ can be accurately measured. The effect of the noise is more dramatic when the line is also broadened by macroturbulence; in this case, most of the power occurs at low frequencies in the Fourier domain and the noise level is above the signal transform even for the first rotational zero. Consequently, the unambiguous identification of the first zero in the Fourier transform becomes difficult or impossible, depending on the combination of $v \sin i$, $v_{\rm m}$ and SNR.

A similar behavior will occur for the H , He I, and He II lines. Although, in principle, it is possible to use these lines to derive the $v \sin i$ (as shown above), since these lines are broadened by mechanisms other than rotation, the signatures corresponding to this rotational broadening may be hidden below the noise level due to the lowering of the low-frequency power caused by Stark broadening.

To obtain an estimation of the feasibility of the FT method when different quality (SNR) spectra are considered, we constructed a grid of synthetic Si III λ 4552 lines convolved with various values of $v \sin i$ and $v_{\rm m}$ and degraded to different SNR values. The FT method was then used to determine the $v \sin i$ for the different cases (see results summarized in Table 1). Although we do not expect the noise to systematically affect the position of the zeroes, this academic example should allow us to better understand the applicability limits of the FT method in real spectra.

In our formal study, we found that the effect of decreasing the SNR is to produce somewhat higher $v \sin i$ values when combined with macroturbulence. Although this effect is not very important when the macroturbulence value is low, deriving correct

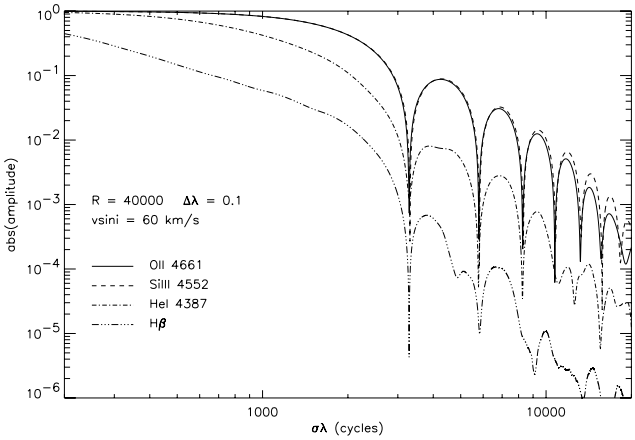

Fig. 1. Four different synthetic line profiles generated with FASTWIND were convolved with a $v \sin i$ of 60 km s^{-1}. The different lines show the FT of the lines on a $\sigma\lambda$ baseline. The first zero fits perfectly to its theoretical value for all the lines. The FT can detect the $v \sin i$ feature even for the He I λ4387 and H$_\beta$ lines. Note that the FT of the H line reaches the value of 1 for $\sigma\lambda < 200$.

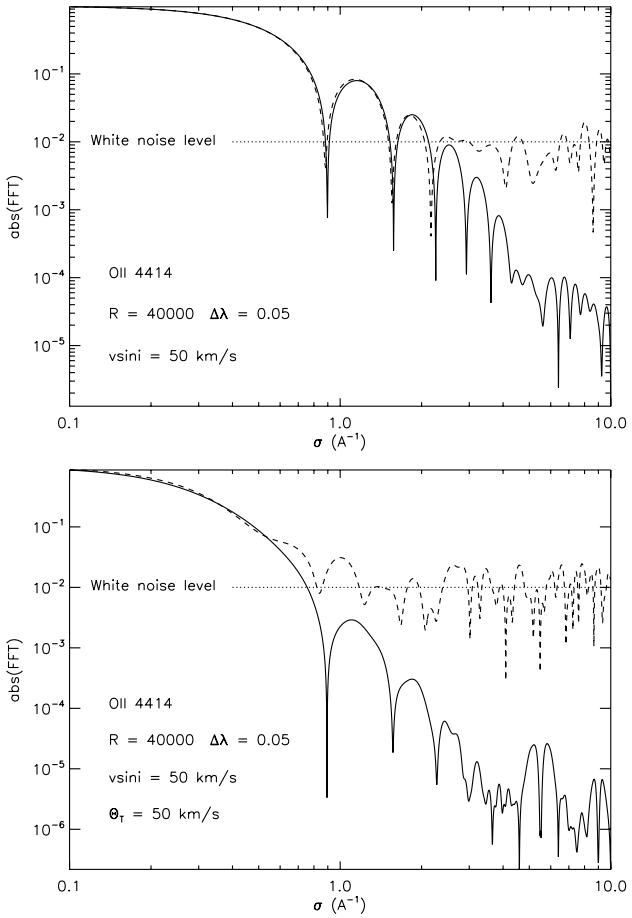

Fig. 2. Effect of the noise on the Fourier transform of a line profile. A Poissonian distribution of noise generated with IDL and corresponding to an $SNR = 200$, was added to a synthetic O II line, broadened to a $v \sin i = 50$ km s^{-1} (*top*) or to a combination of $v \sin i = 50$ km s^{-1} and $v_{\rm m} = 50$ km s^{-1} (*bottom*). The figure compares the transforms of the line with and without noise (dashed and solid lines, respectively).

Table 1. Formal study of the effect of noise on the $v \sin i$ determination when a stellar line (Si III λ4452) is also affected by macroturbulence. We limit ourselves to low values because, at higher $v \sin i$, the problem is much less significant.

$v \sin i$ (km s^{-1})		60			30	
$v_{\rm m}$ (km s^{-1})	0	40	80	0	40	80
$SNR = 500$	60	60	64	30	32	35
$SNR = 300$	60	60	67	26	35	47
$SNR = 100$	62	66	75	32	46	47
$SNR = 50$	59	65	—	34	49	60

values even for $SNR \leq 100$, the effect may be more critical when the amount of macroturbulent broadening dominates the rotational broadening. Note that for the case of $v \sin i = 60$ km s^{-1} and $v_{\rm m} = 80$ km s^{-1} a $SNR \geq 300$ is required to be affected by an error of less than ∼10% in determining of the $v \sin i$. Finally, Table 1 shows how critical the effect of noise can be when the $v \sin i$ is low and the amount of macroturbulence is high (f.e. $v \sin i = 30$ km s^{-1} and $v_{\rm m} = 80$ km s^{-1}), a situation that we may expect to find in supergiants.

The final test relates to the effect of microturbulence, which may introduce additional zeroes as mentioned before. This is illustrated in Fig. 3. For this test a rotational velocity of 60 km s^{-1} was adopted. We see that the Fourier transform of the strong

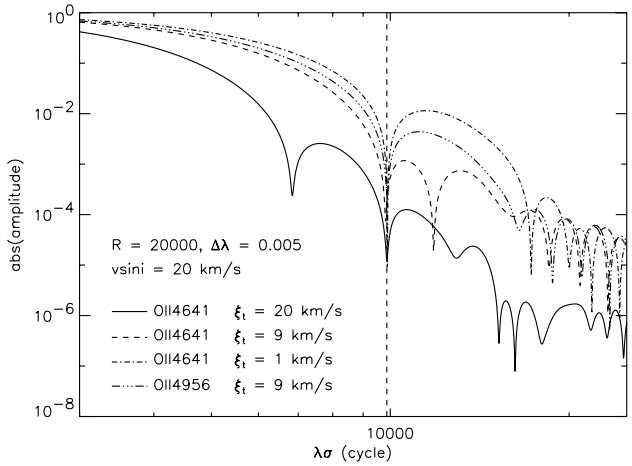

Fig. 3. Effect of the microturbulence on the determination of the $v \sin i$ in Fourier space.

O II λ4641 line presents zeroes that are different when microturbulent velocities of 1, 9, and 20 km s^{-1} are introduced. With only the information from this line, it would be easy to get an incorrect value for the projected rotational velocity when using only the information from the zeroes (particularly if we only use the first one). However, we also see in the figure that we can avoid this error by using the information from weaker lines, like O II λ4956. This line is not significantly affected by the microturbulence, and thus only the zeroes due to rotation are simultaneously present in both transforms.

3. Applying the Fourier method to real OB stellar spectra

In the previous section it has been shown that the FT technique allows us a straightforward determination of projected rotational velocities. When dealing with real spectra, one has to recall two important properties of the FFT algorithm:

1. The sampling of the discrete Fourier transform ($\Delta\sigma$) depends inversely on the product of the number of points into which the line profile is sampled and the spectral dispersion: $\Delta\sigma = (N\Delta\lambda)^{-1}$. Therefore, the better the sampling of the Fourier transform of the line profile, the more accurate the position of the zeroes associated to $v \sin i$ can be determined.
2. The FFT of a sequence of N real numbers is symmetric and hence the maximum σ value that is computed is $\sigma_{\rm max} = (N/2)(N\Delta\lambda)^{-1} = (2\Delta\lambda)^{-1}$, also known as the Nyquist frequency. From formula 1 and this computational property of the FFT, it is found that the spectral dispersion ($\Delta\lambda$) of the stellar spectrum imposes a limit in the lowest $v \sin i$ that can be derived, given by $1.320\,c\,\Delta\lambda/\lambda$. Figure 4 illustrates the minimum $v \sin i$ that can be measured for various characteristic $\Delta\lambda$ values.

Therefore, if the spectrum has enough resolution it will be possible to determine the projected rotational velocity of the star independently of any other broadening mechanism affecting the line profiles. The applicability of the FT method in real spectra is mainly limited by the spectral dispersion (for low $v \sin i$ cases) and the *SNR* (mainly affecting those stellar lines broadened by a non-rotational broadening mechanism, i.e. macroturbulence and/or Stark broadening).

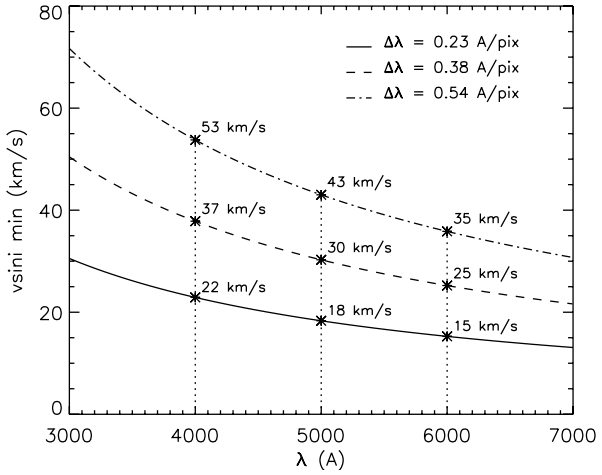

Fig. 4. Minimum $v \sin i$ that can be determined at different wavelengths for various spectral dispersions as a consequence of the combination of formula (1) with the Nyquist frequency.

With these ideas in mind, a sample of stellar spectra of OB stars, obtained during various observing runs, was restored from our archive to determine their projected rotational velocities by means of the FT method. The derived values were compared with those from using the FWHM method. This allowed us to test the validity of the FT method by studying those cases in which stellar lines are broadened mainly by rotation, as well as the range of applicability of the FWHM method. Likewise, the possible presence of macroturbulence could be studied.

3.1. The FWHM method

The FWHM method requires an unbroadened line template that is convolved with rotational profiles corresponding to various $v \sin i$ values. Several authors have considered different possibilities for the unbroadened profiles, from sharp-lined stars observed with the same configuration as the unknowns (see Slettebak 1956, who used 10 Lac; Penny 1996, who used HD 34078; and Howarth et al. 1997, who used τ Sco), to synthetic lines from stellar atmosphere code calculations (e.g. Slettebak et al. 1975, Conti & Ebbets 1977), or even Gaussian profiles with the same EW as the observed line (see Herrero et al. 1992). By determining the FWHM from a Gaussian fit to the rotationally broadened line templates, an FWHM - $v \sin i$ calibration is then generated[2]. In this study we considered the same approach as Herrero et al. (1992).

3.2. The observations

We have selected a sample of Galactic OB stars from observations carried out with the Isaac Newton 2.5 m and the William Herschel 4.2 m telescopes at the Observatorio de El Roque de los Muchachos during various observational campaigns between 1989 and 2003. The Intermediate Dispersion Spectrograph (IDS) and the medium-resolution ISIS spectrograph attached to these telescopes were used. The characteristics of the different observing runs are summarized in Table 2, where the first column identifies the campaign by telescope and year, second column gives the observation date, and the different instrument configurations used in each campaign, along with their spectral dispersion, approximate resolution, and observed spectral range, are specified in columns third to sixth, respectively.

The spectra were selected to have $SNR \geq 200$ and spectral dispersion $\leq$0.4 Å/pix (which implies a minimum $v \sin i$ of $\sim$30−40 km s^{-1}, see Fig. 4). Some spectra were selected to have a SNR slightly below 200 only for late O-type and early B-type dwarfs, as these targets are not expected to be affected by macroturbulence, and hence the effect of noise is less critical when applying the FT method to metal lines. The sample of stars ranges in spectral types from O3 to B2, including dwarfs, giants, and supergiants (see Tables 3 to 9 and Table 10).

The characteristics of the optical spectra of OB stars do not make it possible to use the same set of stellar lines to determine the projected rotational velocities for the whole sample of OB stars. For example, while in late O-type and early B-type stars many metal lines from different elements are present in the stellar spectra, along with H and He I lines, for the earliest O-type stars the spectrum is mainly dominated by H and He II lines, and only a few faint metal lines can be found. Therefore we decided to perform the study separately following the classification presented in Sects. 3.3 to 3.6.

3.3. Early B and late O dwarfs: an easy task

Early B and late O dwarfs have many strong metal lines, along with some He I lines, useful to infer the stellar $v \sin i$. We do not expect important broadening mechanisms other than rotation affecting the metal lines; however, the He lines are additionally broadened by the Stark broadening.

Table 3 show the $v \sin i$ derived from several He I, Si III, C II, N II, and O II lines present in the spectra of dwarf stars with spectral types between B1 and O9 and $v \sin i$ values below 100 km s^{-1}. Results obtained through both the FT and FWHM methods are presented, where values in brackets represent FWHM results. Mean values for He I and metal lines are also presented, with errors showing the standard deviation of line values. For those cases with $v \sin i$ above 100 km s^{-1}, the high $v \sin i$ makes metal lines to be faint and blended, and hence not suitable to measure projected rotational velocities. Except for a few metal lines, only He I lines can be used (see Table 4).

A comparison of $v \sin i$ results is shown in Figs. 5 to 7. For dwarfs, three main conclusions arise from this comparison:

- He I lines give results consistent with metal lines when analyzed with the FT method (Fig. 5, left), but tend to produce higher values for the projected rotational velocities when using the FWHM method (10−20%, see Fig. 5, right).
- From Fig. 6 it can be seen that for O9 - B0 dwarfs both the FT and FWHM methods give similar results when metal lines are used. However, for very high rotational velocities, when no metal lines can be used, He I lines give $v \sin i$ values that are slightly higher when using the FWHM method than when using the FT, although the effect is weaker than for lower $v \sin i$ (see Fig. 7).
- The shape of the Fourier transform of the metal lines is very close to what results from a pure rotational profile, confirming the absence of important broadening mechanisms other than rotation. This fact allows accurate determination of the $v \sin i$ of late-O and early-B dwarfs even for $SNR \sim 120$.

There are two cases (CygOB2-145, and τ Sco) in which the measurement of $v \sin i$ is limited by the spectral resolution. The $v \sin i$ value resulting from the FT analysis is very close to the limit

[2] Note that there is also the possibility of generating a FWHM - $v \sin i$ calibration based in previous $v \sin i$ determinations (cf. Abt et al. 2002; Strom et al. 2005).

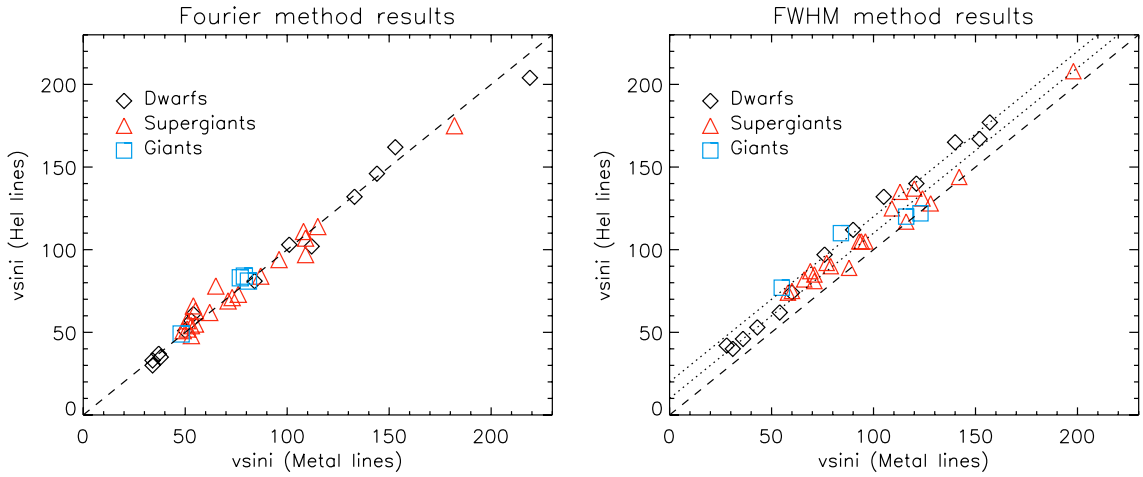

Fig. 5. Comparison of $v \sin i$ results derived from metal and He I lines through the FT and FWHM methods. Only those cases in which $v \sin i$ could be derived through metal lines are presented. Dotted lines in the FWHM diagram represents a difference between both determinations of 10 and 20 km s^{-1}.

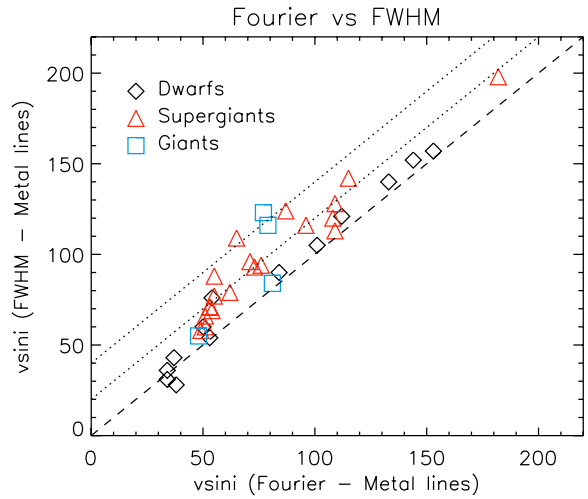

Fig. 6. Comparison of $v \sin i$ results derived from metal lines through the FT and FWHM methods. Dotted lines represent differences between both determinations of 20 and 40 km s^{-1}.

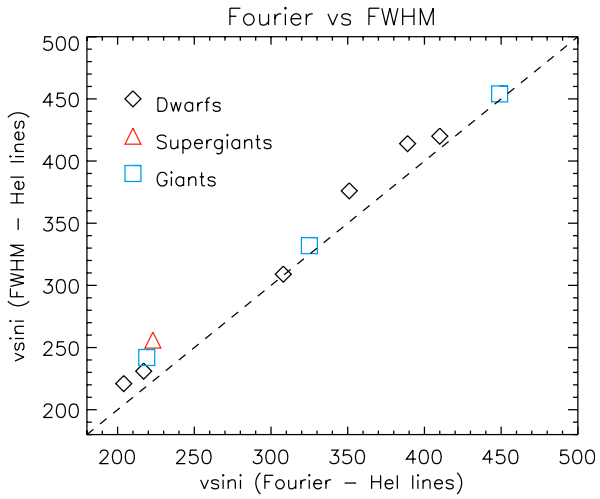

Fig. 7. Comparison of $v \sin i$ results derived from He I lines through the FT and FWHM methods for $v \sin i \geq 180$ km s^{-1}. In this range of projected rotational velocities, no metal lines are accessible for the $v \sin i$ determination.

imposed by the Nyquist frequency (i.e. $1.320\, c\Delta\lambda/\lambda$). In addition, the $v \sin i$ derived from the FWHM method is somewhat below the FT value. A larger spectral dispersion ($\Delta\lambda$) is needed for these stars to correctly derive the $v \sin i$ through the FT method. Moreover, even with higher resolution spectra, the broadening produced by microturbulence may be comparable to the one corresponding to the rotational velocity, so that zeroes associated with microturbulence may be found at frequencies somewhat lower than σ_1 in the Fourier space. These stars may be good examples for studying the effects illustrated in Fig. 3.

Although we are not going to treat it here in detail, we would like to mention that some studies have shown that in the cases of high $v \sin i$, the effect of differential rotation may alter the position of zeroes in the Fourier transform. We refer the reader to Reiners & Royer (2004) for a detailed study of this effect in the case of A-type stars. However, note that Reiners & Royer only find evidence of differential rotation in 4 out of 78 stars of spectral types later than ours, so we do not expect this effect to be important in our sample.

3.4. Early B and late O supergiants: the presence of extra broadening

The logical extension of the previous analyses points towards early B and late O supergiants, since these stars also have many narrow metal lines. Results for a sample of supergiants with spectral types ranging from O9 I to B2 I are presented in Table 5, and in Figs. 5 to 7, the results from both the FT and FWHM methods are again compared.

In the case of supergiants we find:

- The FT method again gives consistent results for both metal and He I lines (Fig. 5).
- For metal lines, the $v \sin i$ derived through the FWHM method is systematically higher than from the FT method (Fig. 6). This result confirms the presence of an extra broadening mechanism in early B-type supergiants, as shown by Dufton et al. (2006a), and extends the results towards late O-type supergiants.
- An additional indication of extra broadening is clearly shown by the shape of the Fourier transform of metal lines (see e.g.

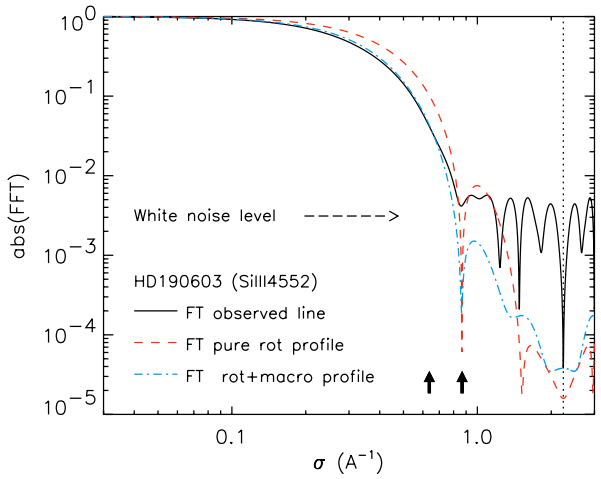

Fig. 8. Fourier transform of the Si III λ4552 line in the ISIS@WHT spectrum of HD 190603 (B1.5Ia$^+$). The FT of the observed line (solid black) is compared with two synthetic profiles: (dashed red) pure rotational profile with $v \sin i = 50$ km s^{-1}; (dashed-dotted blue) rotational + macroturbulent profile with $(v \sin i, v_{\rm m}) = (50, 45)$ km s^{-1}. Black arrows show the position of the zeroes associated with $v \sin i$ values of 50 and 68 km s^{-1}, corresponding to the values derived through the FT and FWHM methods, respectively.

Fig. 8). In this case, the power of the Fourier transform concentrates at higher frequencies when compared to the Fourier transform of a pure rotational line profile with the same EW.

In Sect. 2.1 it was shown that the effect of the white noise in Fourier space can be important when extra-broadening is present. If the *SNR* of the spectrum is not good enough, the zeroes associated to the $v \sin i$ may be hidden below the white noise and may be mistaken for artificial zeroes associated with this white noise (see Fig. 2). A low *SNR* may result in higher $v \sin i$ derived values.

In Fig. 8, the line Si III λ4552 in the ISIS@WHT spectrum of HD 190603 (B1.5Ia$^+$) is used to illustrate the application of the FT method to an early B-type supergiant. The spectrum has an *SNR* ~ 570 (see Table 5). The position of the first zero in the FT of the observed line corresponds to a $v \sin i = 50$ km s^{-1}. The shape of the FT of a pure rotational (+ instrumental!) profile corresponding to that value does not fit the observed case correctly for low frequencies. An extra macroturbulent broadening, $v_{\rm m}$, is needed to produce a satisfactory fit in Fourier space. Note that in this case the power of the FT is below the white noise level of the observed line, thus indicating that the FT of the observed profile may be affected by the white noise, even for those frequencies where the first zero associated with the rotation is located. The actual $v \sin i$ value may be somewhat lower (and consequently, $v_{\rm m}$ higher).

3.5. Early and mid-O dwarfs and supergiants

When moving to earlier spectral types (mid and early O-type), most of the strong metal lines present in the optical spectra of early B-type stars become very faint or even do not appear anymore. A few lines associated with high ionized states of C, N, O, and Si can be found in mid O-type stars, and a few metal lines in emission are present in the spectra of the earliest spectral types. In contrast, the spectra of mid O-type stars are dominated by strong He I and He II lines. And finally, even He I lines become weak for the hottest stars. Therefore, in the optical spectra of those stars, only a few He lines are available for the $v \sin i$ determination.

In previous sections, it has been shown that He I lines result in somewhat higher $v \sin i$ values than metal lines when measured with the FWHM method. In contrast, the FT method produces excellent agreement. Therefore, application of the FT method to the He I lines in O-type stars is very promising for deriving reliable $v \sin i$ values.

It is important to note that *SNR* imposes a strong limitation when the FT method is applied to He I lines. Since the Stark broadening mechanism has a big influence on the He I lines, high *SNR* spectra are necessary to be sure that white noise in the Fourier space is not affecting the identification of the first rotational zero (as shown in Sect. 2.1). The effect of noise may be even more dramatic if macroturbulence is also affecting the He I line profiles. However, note that macroturbulent broadening is expected to be greater in giants and supergiants, while Stark effect in these stars contributes less to the broadening of the He I lines (i.e. Stark broadening scales roughly as ρ^2). Note also that, although the spectra of early O-type stars show quite large He II lines, the effect of Stark broadening is stronger for these lines than for He I lines. Therefore, considering the comment above, the use of these lines will require spectra with a very high *SNR*. We did not achieve enough *SNR* in any of the spectra of our sample of early O-type stars, so He II could not be used.

Tables 6 and 7 summarize the line-to-line $v \sin i$ values resulting from the FWHM and FT analyses of the sample of early and mid O-type dwarfs and supergiants. The He I lines were mainly used; however, for the supergiants, we could also use some metal lines, which some of them present in the spectral range between 5000 and 6000 Å, only observed in the WHT03 campaign. A comparison of $v \sin i$ results is again shown in Figs. 5 to 7.

From the comparison of $v \sin i$ values obtained for metal lines with the FT and FWHM methods in some of the supergiants in our sample, we can conclude that macroturbulence is also present in these stars, extending the result found in B-type supergiants to the O-type supergiants. Unfortunately, the presence of macroturbulence in the early O-type dwarfs could not be investigated because there were no metal lines available for the $v \sin i$ determination.

3.6. OB giants

Results for the determination of projected rotational velocities in the sample of giant stars are presented in Tables 8 and 9. Similar to previous sections, $v \sin i$ measurements from both the FT and FWHM for several lines, as well as mean values for He I and metal lines, are summarized there. We mainly used He I linesfor these stars, although a few Si IV, C IV, N II and O III lines were also available in some cases.

The analysis of the sample of Giant stars points towards two curious results:

- both low and high $v \sin i$ values are found;
- the macroturbulent effect is either very strong or negligible.

These will be discussed in more detail in the next section.

4. Discussion

Figure 5 shows a comparison of $v \sin i$ results obtained for the sample of stars when applying the FT and FWHM methods to metal and He I lines. This comparison was only possible for stars

with $v \sin i$ values below 200 km s^{-1}. For those cases with a projected rotational velocity above this value metal lines appeared blended or very faint, so they were not available for deriving $v \sin i$. For the studied stars, the FT method produces coherent results between metal and He I lines, indicating the possibility of accurately deriving projected rotational velocities by this method by using He I lines. This is not the case for the FWHM method, whose He I lines $v \sin i$ associated values are somewhat higher than those derived from metal lines, even for high values of $v \sin i$ (see also Fig. 7). This result is a consequence of the He I lines being affected by Stark broadening, while we are considering a Gaussian definition of the intrinsic profiles. It indicates that the assumption made by Herrero et al. (1992) that this hypothesis can be used when applying the FWHM method to He I lines for determining $v \sin i$ if this is high, is not completely correct. The effect of pressure broadening over He I may be important even for high projected rotational velocities, although for $v \sin i > 250$ km s^{-1} the relative error is small. Note that, although this discrepancy should not be present if the intrinsic profiles used for the He I lines consider the Stark broadening, the derived FWHM values may require much computational effort and be model-dependent, while FT values will not.

Since the Stark effect over the He I lines scales roughly as ρ^2, these lines are expected to be less affected by Stark broadening in supergiants. This explains why for some of the studied supergiants, a better He I vs. metal lines agreement is found when applying the FWHM method (Fig. 5, right). However, be careful, as the agreement between He I and metal lines does not necessarily mean that the FWHM method is giving correct values for the $v \sin i$.

Differences between the $v \sin i$ values obtained by applying the FWHM and FT methods to metal lines can be interpreted as an indicator of the presence of some extra broadening, traditionally associated to large-scale motions. As indicated above, we refer to it as macroturbulence. This is illustrated in Fig. 6. The whole sample of stars whose metal lines are available for the $v \sin i$ to be measured are considered in this figure. Note that a similar comparison with He I lines (i.e. Fig. 7) does not make sense for investigating the presence of macroturbulence using the differences between the FT and FWHM methods, since these lines are also affected by other non-rotational broadenings, as shown above. Metal lines are also affected by other line broadening mechanisms, like thermal or collisional ones, but we expect them to be negligible, as shown by the agreement found in dwarf analyses. Stars have been separated according to luminosity class. While macroturbulence can be considered negligible in dwarfs, supergiants are clearly affected by this extra-broadening mechanism; 65% of the sample of supergiants shows $v \sin i$ (FT) ≤ 0.8 $v \sin i$ (FWHM). The case of giants is more complicated; these objects display a wide range of $v \sin i$(FT)/$v \sin i$(FWHM) ratios.

Supergiants rotate as a group more slowly than dwarfs do. Except for two cases among early O-type supergiants (CygOB2-8C and HD 218039), all of them have projected rotational velocities below or very close to 100 km s^{-1}. This has to be compared with the wide range of $v \sin i$ found for dwarfs and giants, which covers from about 15 up to 450 km s^{-1}. In Fig. 9 we see that the region of low rotational velocities is shared by all spectral types and luminosity classes, but that of high rotational velocities is dominated by giants and dwarfs of mid and late spectral types. This result has already been indicated by Slettebak (1956) and later on by other authors (viz. Conti & Ebbets 1977; Howarth et al. 1997). These authors also propose indirect indications of the possible presence of

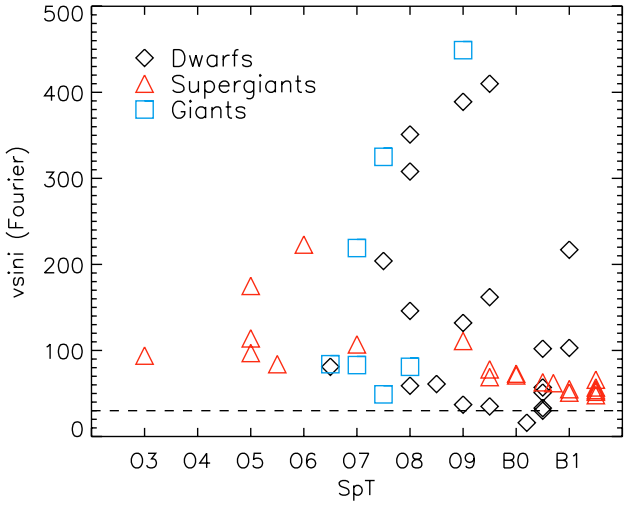

Fig. 9. Distribution of projected rotational velocities (as determined by the FT method) among the various spectral types of the stars in the sample. Both $v \sin i_{\rm FT}$(metal) and $v \sin i_{\rm FT}$(He I) are used in this figure. The horizontal dashed line represents the resolution limit for $R = 9000$.

macroturbulence in OB stars, but could not directly confirm the amount of broadening that is actually due to rotation, and therefore their $v \sin i$values are affected by the contribution of macroturbulence. The FT method shows that indeed very high rotational velocities are the cause of the large line broadening in dwarfs, and allows for a quantitative estimation of the actual $v \sin i$ in supergiants (where effects of macroturbulence are important). First results for a more limited sample were presented by Ebbets (1979). Our results also support the bimodality found by Conti and Ebbets (1977) and other authors in the $v \sin i$ distribution of main sequence stars.

Although it is clear that supergiants are affected by macroturbulence, our knowledge of its behavior and the physical mechanisms that produce this extra broadening is still very poor. In Sect. 2.1 an isotropic Gaussian macroturbulence was assumed for the formal tests; however, as shown by Dufton et al. (2006a), one cannot rule out other macroturbulent velocity distributions from the comparison with high-resolution observed line profiles. Physically, a Gaussian-angle-dependent velocity distribution similar to the one proposed by Gray (1976) to model the flow of convective cells in the Sun may also make sense in the case of B supergiants. In that case, the large-scale radial-tangential movements may be produced when the stellar material flowing outwards as a stellar wind is coupled with the stellar rotation. Observational tests to investigate the exact degree of the anisotropy of the macroturbulence should be investigated in the future. In the meantime, rough estimations of the macroturbulence are also valuable, once the projected rotational velocity has been inferred. Note that the characteristic value of the macroturbulent velocity is dependent on the approach considered for the macroturbulent velocity distribution (see p.e. Dufton et al. 2006a).

The quality of our observational dataset (mainly selected to show the applicability of the FT method to OB stars) is not good enough to proceed to a fine estimation of the macroturbulence[3]. However, taking the discussion above into account, we decided to consider a rough estimation of the amount

[3] We refer to the works by Dufton et al. (2006a) and Lefever et al. (2006) as examples of macroturbulent determination through better-quality observational data.

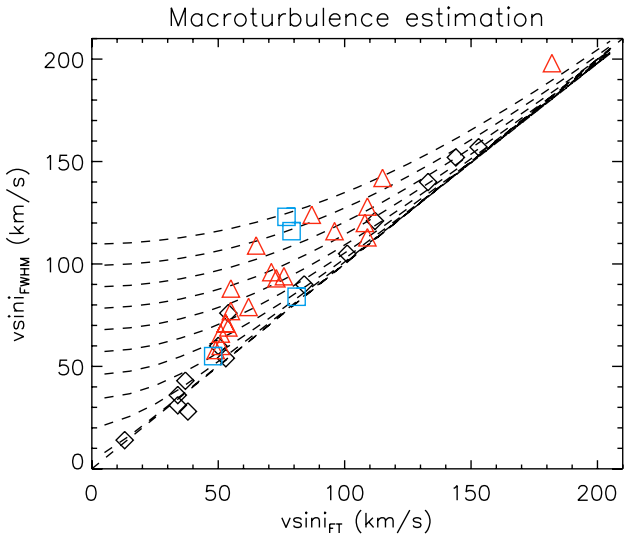

Fig. 10. This plot illustrates the method used to derive Θ_0, a rough estimation of the macroturbulence. The various dashed curves represent cases with different values of Θ_0, from 5 to 95 km s^{-1}. An instrumental profile (R = 9000) has also been considered (see text for explanation). Symbols have the same meaning as in previous figures.

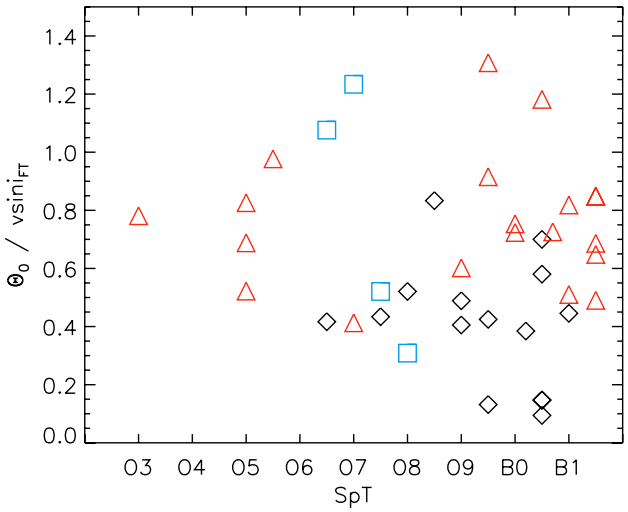

Fig. 11. Distribution of the ratio $\Theta_0/v \sin i$ in the sample of stars as a function of spectral types. Only those stars with metal lines available to measure $v \sin i_{FW}$ and $v \sin i_{FT}$ were used (see text and Fig. 10).

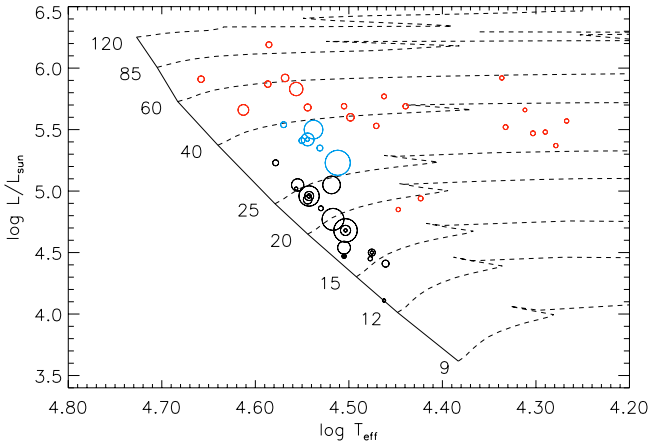

Fig. 12. HR diagram where the stars in the studied sample have been located with symbol sizes proportional to their rotational ($v \sin i_{FT}$) velocities. As in previous figures, black, blue, and red symbols represent dwarfs, giants and supergiants, respectively.

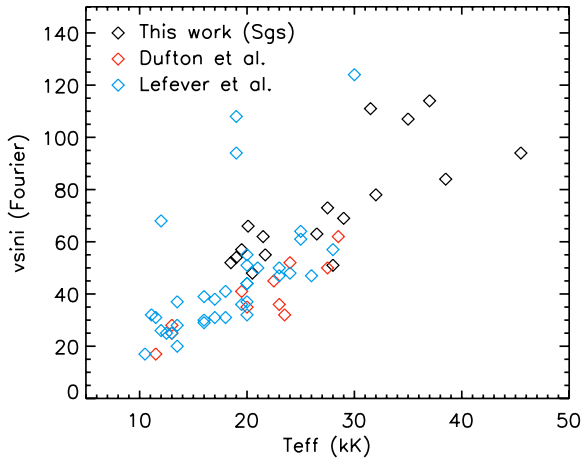

Fig. 13. Estimates of projected rotational velocities for our sample of supergiant stars. Results from the analysis of the Galactic B-type supergiants by Dufton et al. and Lefever et al. are also included.

of extra-broadening, given by Θ_0, where this quantity is calculated as follows. A $v \sin i$-FWHM calibration is created by measuring the FWHM corresponding to the convolution of an instrumental profile and various values of $v \sin i$. This calibration is applied to a second set of line profiles in which an isotropic Gaussian macroturbulence (with characteristic velocity Θ_0) is also included. The corresponding $v \sin i_{FWHM}$ is hence inferred for various $v \sin i$ - Θ_0 combinations, ending with a set of lines in the $v \sin i_{FWHM}$ - $v \sin i_{FT}$ plane (see Fig. 10). Once these two quantities are measured for a given star, the Θ_0 can be estimated by interpolation between these curves. We expect the quantity Θ_0 calculated in this way to be roughly proportional to the macroturbulent velocity and to behave in a similar way when varying the stellar parameters.

The influence of Θ_0 relative to $v \sin i$ seems to increase when moving from dwarfs to supergiants, as can be seen in Fig. 11. We decided to plot $\Theta_0/v \sin i$ vs. SpT, instead of Θ_0, because for high values of $v \sin i$ it is more difficult to distinguish between the different values of Θ_0, as illustrated by the proximity of the dashed curves when $v \sin i$ increases. We consider this ratio more meaningful.

Except for the two giants around O7, the highest values at each spectral type are always obtained for supergiants. Only two dwarfs have $\Theta_0/v \sin i$ comparable to the one found in supergiants: HD 37023, which is known to be binary, and HD 168137 (O8.5 V).

Combining both results, we conclude that the role of rotation should decrease and the role of macroturbulence increase when the stars move from dwarfs to supergiants, i.e., when they evolve. This can also be seen in Figs. 12 and 13, where we represent the stars on a HR diagram, with symbol sizes proportional to their rotational and macroturbulent velocities. To place the stars in the HRD we have taken results from various authors that used state-of-the-art NLTE, line-blanketed, unified model atmospheres (Herrero et al. 2002; Repolust et al. 2004; Urbaneja 2004; Simón-Díaz 2005; Simón-Díaz et al. 2006; Crowther et al. 2006). For those stars in the sample that have not been previously analyzed, we used the SpT-T_{eff} and SpT-L calibrations defined by Martins et al. (2005). Note that for some of the B0.5V

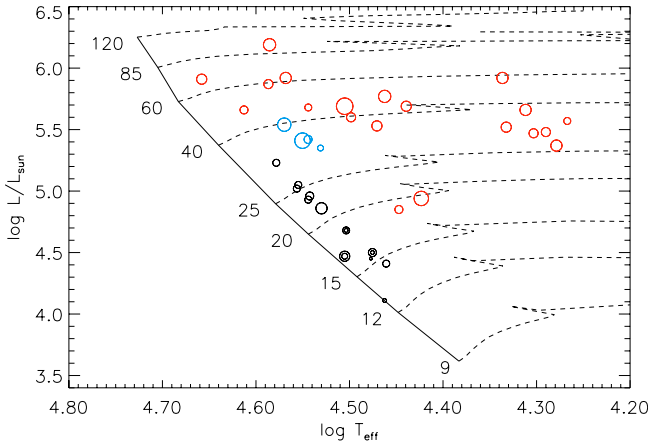

Fig. 14. Same as in Fig. 12 but for the quantity Θ_0 (i.e. rough estimation of the macroturbulence).

stars, the stellar parameters were obtained by extrapolating the calibration by Martins et al.

We see that the symbols in Fig. 12 may have any size close to the ZAMS, but they become smaller when we depart from it. Beyond an imaginary line parallel to the ZAMS, all symbols are very small, indicating slow rotation. Although the inclination angle is unknown, it is obvious that the effect cannot be attributed to a random effect. Clearly, all supergiants have low rotational velocities which, in view of the distribution for dwarfs and giants, indicates that the stellar rotational velocities decrease when the stars evolve. As suggested by other authors (see review by Herrero & Lennon 2004), this may be related to the loss of angular momentum caused by stellar winds.

Recently Dufton et al. (2006a) and Lefever et al. (2006) have applied the FT method to two samples of Galactic B-type supergiants observed with high spectral resolution. They found higher $v \sin i$ values for the earliest spectral types. We put together the $v \sin i$ results by these authors and our results in Fig. 14. We can see that they agree very well and that our results extend those of Dufton et al. and Lefever et al. towards higher temperatures.

Additionally, these authors could use the good quality of their data to estimate the amount of macroturbulent broadening present in the stars by means of the fit of the theoretical line profiles to the observed ones. Since we limit ourselves to a crude first-order approximation as shown above, we have to be very careful when interpreting the results concerning our estimation of what we have called macroturbulence[4]. However, it is interesting to see how this estimation varies across the HR diagram. In Fig. 13 we see that the symbol sizes representing the macroturbulent velocity have a much more uniform distribution than those of the rotational velocities, with the lowest values corresponding to dwarfs close to the ZAMS. Part of this difference may be related to projection effects (that would affect large scale turbulent motions much less than rotation). Nevertheless, according to these estimations, macroturbulence does not necessarily increase significantly when the stars evolve redwards, but may remain approximately constant. However, its role in line broadening relative to rotation increases (and perhaps also in other physical mechanisms). Note that the broad scenario suggested here (rotational velocity decreasing when the stars evolve from dwarfs to supergiants, macroturbulence being roughly constant but taking a dominant role) has been deduced from the study of a very inhomogeneous sample of OB stars. To better understand the role that rotation and macroturbulence play in the evolution of massive stars, a homogeneous study of stars in clusters of different ages and metallicities should be performed (viz. Dufton et al. 2006b; Mokiem et al. 2006).

[4] Note that even a comparison of the values inferred by these authors for the macroturbulence should be handled with care, since Dufton et al. use an isotropic Gaussian definition, while Lefever et al. assume a radial-tangential approach.

5. Conclusions

In the past the Fourier method of determining projected rotational velocities has been extensively used in the analysis of late-type stars, but only marginally applied to the early-type case. In this paper we show the strength of this method for its application to OB stars.

The noise and the spectral dispersion of the observed spectra are the main limitations to the Fourier method. Spectral dispersions below 0.4 Å/pix are required to measure $v \sin i$ values below 30−40 km s^{-1} when using the optical spectrum of OB stars. For dwarf stars, which are not very affected by non-rotational broadenings (i.e. macroturbulence), the FT method can be successfully applied even for *SNR* values as low as 100. The effect of noise is greater in the case of supergiants, where absorption stellar lines are broadened by other mechanisms than rotation. If the *SNR* of the observed spectra is not high enough and the amount of macroturbulent broadening is close to rotational broadening, the application of the FT may result in somewhat higher $v \sin i$ values than the actual ones; *SNR* values above 300−400 are required for these cases.

The comparison of $v \sin i$ values obtained through the FT and FWHM methods in a sample of O and early-B stars shows that the FWHM technique must be used with care when analyzing OB giants and supergiants and when it is applied to He I lines. In contrast, the FT method appears to be a powerful tool for deriving reliable projected rotational velocities and separating the effect of rotation from other broadening mechanisms present in these stars.

The analysis of the sample of OB stars, which includes dwarfs, giants and supergiants with spectral types earlier than B2, shows that while dwarfs display a broad range of projected rotational velocities, from less than 30 up to 450 km s^{-1}, supergiants generally have values close to or below 100 km s^{-1}. Giants also display a wide range of projected rotational velocities. The analysis has also definitely shown that, while the effect of macroturbulence in OB dwarfs is usually negligible when compared with the rotational broadening, the effect of this extra-broadening is clearly present in supergiants.

When examining the behavior of the projected rotational velocities with the stellar parameters and across the HR diagram, we conclude, in agreement with previous researchers, that the rotational velocity should decrease when the stars evolve. On the contrary, extra broadening across the HR diagram, interpreted as macroturbulence, may be constant, resulting therefore in increasing importance as compared to rotation when the stars evolve.

Acknowledgements. We thank C. Trundle for her detailed reading of the first manuscript of this work and for many fruitful discussions and comments. We also thank M.R. Villamariz, J. Puls, D. J. Lennon, and P. Dufton for numerous insightful discussions. We acknowledge the comments by the anonymous referee. This work has been partially funded by the Spanish Ministerio de Educación y Ciencia under project AYA2004-08271-C02-01. S.-D. also acknowledges the funds by the Spanish Ministerio de Educación y Ciencia under the MEC/Fullbright postdoctoral fellowship program.

References

Abt, H. A., Levato, H., & Grosso, M. 2002, ApJ, 573, 359
Bruning, D. H. 1984, ApJ, 281, 830
Carroll, J. A. 1933, MNRAS, 93, 478
Conti, P. S., & Ebbets, D. 1977, ApJ, 213, 438
Crowther, P. A., Lennon, D. J., Walborn, N. R., & Smartt, S. J. 2006, to appear in Mass loss from stars and the evolution of stellar clusters, ASP Conf. Ser., ed. A. de Kotter, L. J. Smith, & R. Walters [arXiv:astro-ph/0606717]
Dufton, P. L., Ryans, R. S. I., Simón-Díaz, S., et al. 2006a, A&A, 451, 603
Dufton, P. L., Smartt, S. J., Lee, J. K., et al. 2006b, A&A, 457, 265
Ebbets, D. 1979, ApJ, 227, 510
Gray, D. F. 1973, ApJ, 184, 461
Gray, D. F. 1975, ApJ, 202, 148
Gray, D. F. 1976, The observation and analysis of stellar photospheres (Cambridge: Cambridge Univ. Press)
Gray, D. F. 1980, PASP, 92, 771
Gray, D. F. 2005, The observation and analysis of stellar photospheres (Cambridge, Cambridge University Press) 3rd edn.
Herrero, A., Kudritzki, R. P., Vilchez, J. M., et al. 1992, A&A, 261, 209
Herrero, A., Puls, J., & Najarro, F. 2002, A&A, 396, 949
Herrero, A., & Lennon, D. J. 2004, IAUS, 215, 209
Howarth, I. D., Siebert, K. W., Hussain, A. J., & Prinja, R. K. 1997, MNRAS, 284, 265
Lefever, K., Puls, J., & Aerts, C. 2007, A&A, 463, 1093
Maeder, A., & Meynet, G. 2000, ARA&A, 38, 143
Maeder, A., & Meynet, G. 2001, A&A, 373, 555
Martins, F., Schaerer, D., & Hillier, D. J. 2005, A&A, 436, 1049
Mihalas, D. 1979, MNRAS, 189, 671
Mokiem, M. R., de Koter, A., Evans, C. J., et al. 2006, A&A, 456, 1131
Penny, L. R. 1996, ApJ, 463, 737
Penny, L. R., Sprague, A. J., Seago, G., & Gies, D. R. 2004, ApJ, 617, 1316
Puls, J., Urbaneja, M. A., Venero, R., et al. 2005, A&A, 435, 669
Repolust, T., Puls, J., & Herrero, A. 2004, A&A, 415, 349
Reiners, A., & Schmitt, J. H. M. M. 2003, A&A, 398, 647
Reiners, A., & Royer, F. 2004, A&A, 415, 325
Ryans, R. S. I., Dufton, P. L., Rolleston, W. R. J., et al. 2002, MNRAS, 336, 577
Royer, F., Gerbaldi, M., Faraggiana, R., & Gómez, A. E. 2002a, A&A, 381, 105
Royer, F., Grenier, S., Baylac, M.-O., et al. 2002b, A&A, 393, 897
Santolaya-Rey, A. E., Puls, J., & Herrero, A. 1997, A&A, 323, 488
Simón-Díaz, S. 2005, Ph.D. Thesis, Univ. La Laguna
Simón-Díaz, S., Herrero, A., Esteban, C., & Najarro, F. 2006, A&A, 448, 351
Slettebak, A. 1956, ApJ, 124, 173
Slettebak, A., Collins II, G. W., Boyce, P. B., et al. 1975, ApJSS, 281, 29, 137
Smith, M. A. 1976, ApJ, 208, 487
Smith, M. A., & Gray, D. F. 1976, PASP, 88, 890
Strom, S. E., Wolff, S. C., & Dror, D. H. A. 2005, AJ, 129, 809
Urbaneja, M. A. 2004, Ph.D. Thesis, Univ. La Laguna

Online Material

Table 2. Observations used for the present work.

Obs. C.	Date	I. config.	$\Delta\lambda$ (Å/pix)	R	λ coverage
INT89	Jul. 1989	IDS235 - H2400B	0.38	7500	4000–5000 Å
INT92	Sept. 1991	IDS235 - H2400B	0.23	9000	4000–5100 Å
	—	IDS235 - H1800V	0.23	9000	6500–6700 Å
WHTB		ISIS - R1200B	0.23	9000	4000–4750 Å
INT02	Dec. 2002	IDS235 - H2400B	0.23	9000	4050–5100 Å
	—	IDS235 - H1800V	0.23	9000	6500–6700 Å
WHT03	Jun. 2003	ISIS - R1200B	0.23	9000	3900–5100 Å
	—	ISIS - R1200B	0.23	9000	5500–5900 Å
	—	ISIS - R1200B	0.23	9000	6500–6700 Å
CASPEC		CASPEC@ ESO3.6	0.10	18000	4050–5000 Å

Table 3. Projected rotational velocities ($v \sin i$ in km s^{-1}) for the dwarf stars with spectral types between B1 and O9. (b) blended line, (r) noise important, (d) faint line, (-) line not present in the observed spectrum (either because that line does not appear for this SpT, or because it is out of the observed spectral range).

Star	ω^1 Sco	HD 217657	HD 37020	HD 37023	HD 37042	τ Sco	CygOB2-145	HD 214680
SpT	B1V	B0.5V	B0.5V	B0.5V	B0.5V	B0.2V	O9.5V	O9V
Obs. run	WHT03	INT92	INT02	INT02	INT02	CASPEC	WHT03	WHT03
SNR	350	120	220	290	350	250	120	
He I λ 4713	102 (115)	31 (38)	53 (58)	50 (69)	31 (46)	14 ( )	35 (35)	36 (48)
He I λ 4922	104 (178)	b	b	b	b	b	b	b
He I λ 5015	101 (114)	29 (35)	60 (63)	48 (77)	30 (45)	15 ( )	28 (34)	35 (50)
He I λ 5047	102 (125)	32 (36)	52 (55)	52 (70)	32 (39)	18 ( )	28 (30)	33 (46)
He I λ 5875	104 (119)	-	-	-	-	-	48 (59)	47 (64)
He I λ 6678	105 (120)	29 (49)	62 (70)	55 (80)	35 (53)	-	34 (50)	36 (58)
Si III λ 4552	101 (110)	36 (21)	56 (56)	52 (72)	32 (36)	10 (13)	40 (27)	34 (40)
Si III λ 4567	104 (110)	31 (33)	49 (58)	50 (69)	33 (37)	12 (14)	41 (20)	38 (46)
Si III λ 4574	103 (114)	39 (35)	53 (54)	54 (70)	31 (33)	11 (13)	39 (24)	32 (43)
C II λ 4267	97 (100)	41 (36)	49 (53)	54 (75)	32 (37)	21 (22)	36 (38)	40 (44)
N II λ 3995	103 (102)	44 (28)	-	-	-	-	-	45 (49)
N II λ 4253	96 (99)	43 (44)	56 (60)	55 (66)	36 (44)	b	43 (36)	38 (50)
N II λ 4601	104 (110)	r	53 (50)	54 (62)	b?	b	d	35 (42)
O II λ 4317	b	36 (35)	56 (54)	51 (55)	37 (38)	14 (12)	44 (31)	d
O II λ 4319	b	36 (36)	58 (54)	47 (53)	38 (35)	12 (14)	39 (25)	39 (42)
O II λ 4414	b	32 (25)	49 (52)	48 (50)	40 (36)	14 (13)	35 (29)	d
O II λ 4416	b	30 (29)	52 (49)	47 (61)	33 (36)	10 (14)	r	d
O II λ 4590	108 (109)	32 (28)	54 (55)	48 (63)	32 (35)	12 (13)	40 (48)	b
O II λ 4595	97 (105)	35 (36)	56 (54)	48 (52)	35 (37)	12 (16)	42 (24)	39 (44)
O II λ 4661	102 (99)	28 (24)	55 (51)	51 (55)	30 (33)	14 (13)	33 (18)	37 (37)
O II λ 4699	b	29 (35)	51 (56)	48 (54)	35 (38)	b	33 (34)	37 (44)
O II λ 4705	b	30 (21)	48 (52)	44 (52)	33 (33)	14 (14)	35 (28)	34 (37)
O II λ 4906	100 (100)	d	57 (52)	46 (51)	40 (37)	16 (12)	d	d
O II λ 4943	b	29 (26)	53 (57)	b	34 (30)	12 (13)	29 (21)	d
$v \sin i$ (FT-He)	103 ± 2	30 ± 2	57 ± 5	51 ± 3	33 ± 4	16 ± 2	35 ± 8	37 ± 6
$v \sin i$ (FW-He)	132 ± 24	40 ± 6	62 ± 7	74 ± 5	46 ± 6	±	42 ± 12	53 ± 8
$v \sin i$ (FT-M)	101 ± 4	34 ± 5	53 ± 3	50 ± 3	34 ± 3	13 ± 3	38 ± 4	37 ± 3
$v \sin i$ (FW-M)	105 ± 5	31 ± 6	54 ± 3	60 ± 8	36 ± 4	14 ± 3	28 ± 8	43 ± 4

Table 4. Same as in Table 3 but for stars with $v \sin i$ values above 110 km s^{-1}.

Star	HD 37061	HD 228199	CygOB2-23	BD-134928	HD 149757	HD 37041
SpT	B1V	B0.5V	O9.5V	O9.5Vn	O9.5Vnn	O9V
Obs. run	INT02	INT89	WHT03	WHT03	WHT03	INT02
SNR	250	100	190	230	500	230
He I λ 4387	213 (235)	109 (146)	158 (185)	404 (433)	360 (440)	132 (180)
He I λ 4471	213 (270)	91 ()	159 (212)	b	377 (433)	141 (200)
He I λ 4713	220 (224)	99 (114)	167 (160)	d	b	127 (145)
He I λ 4922	218 (250)	107 (159)	177 ()	405 (416)	389 (402)	125 (170)
He I λ 5015	216 (206)	-	153 (162)	401 (415)	410 (411)	135 (138)
He I λ 5047	(212)	-	d	d	395 (420)	130 (166)
He I λ 5875	-	-	154 (166)	429 (421)	385 (387)	-
He I λ 6678	220 (219)	-	164 (176)	b	404 (407)	133 (158)
Si III λ 4552	d	114 (116)	d	d	d	d
Si III λ 4567	d	118 (127)	d	d	d	d
Si III λ 4574	d	103 (120)	d	d	d	d
Si IV λ 4089	d	b	153 (157)	b	b	133 (140)
$v \sin i$ (FT-He)	217 ± 3	102 ± 8	162 ± 8	410 ± 13	389 ± 17	132 ± 5
$v \sin i$ (FW-He)	231 ± 23	140 ± 23	177 ± 20	420 ± 8	414 ± 18	165 ± 21
$v \sin i$ (FT-M)	-	112 ± 8	153	-	-	133
$v \sin i$ (FW-M)	-	121 ± 6	157	-	-	140

Table 5. Same as Table 3 but for Early-B and late-O supergiants.

Target	HD 210809	CygOB2-10	HD 209975	HD 167264	HD 37128	HD 38771	HD 2905
SpT	O9I	O9.5I	O9.5Iab	B0Ia	B0Ia	B0.5Ia	BC0.7Ia
Obs. run	INT89	WHT03	INT89	WHTB	WHTB	WHTB	WHTB
SNR	200	250	200	400	330	400	300
C II 4267		r	-	73 (88)	75 (94)	67 (80)	69 (78)
N II 3995		d	-	67 (72)	64? (89)	58 (80)	58 (66)
N II 4254		r	-	75 (94)	69 (92)	57 (89)	64 (83)
N II 4601		-	-	-	81 (91)	59 (89)	72 (81)
N II 4614		-	-	-	-	-	-
N II 4621		-	-	-	-	-	-
N II 4630		79 (80)	69 (71)	65 (89)	-	55 (94)	62 (78)
Si III 4552		63 (93)	r	73 (100)	83 (98)	53 (98)	64 (87)
Si III 4567		76 (101)	r	76 (100)	83 (98)	52 (96)	55 (87)
Si III 4574		81 (99)	r	77 (103)	r (77)	r (94)	52 (81)
Si IV 4089	105 (125)	78 (116)	59 (110)	72 (114)	79 (112)	73 (99)	r (86)
Si IV 4116	110 (115)	72 (93)	70 (108)	(101)	65 (98)	51 (80)	67 (70)
O II 4590		76 (106)	-	75 (92)	81 (94)	51 (86)	66 (81)
O II 4595		r	-	52 (82)	81 (94)	52 (85)	58 (82)
O II 4661		61 (76)	d	73 (82)	74 (96)	53 (86)	55 (81)
He I 4143		r	70 (115)	68 (100)	78 (94)	68 (96)	69 (83)
He I 4387	108 (140)	70 (102)	80 (132)	75 (107)	79 (104)	71 (99)	65 (99)
He I 4471	113 (150)	76 (113)		73 (120)	74 (127)	b	b
He I 4713	111 (127)	61 (93)	75 (117)	65 (88)	67 (85)	55 (78)	59 (81)
He I 4922	110 (130)	76 (114)	-	-	-	-	-
He I 5015	-	60 (98)	-	-	-	-	-
He I 5047	-	61 (85)	-	-	-	-	-
He I 5875	-	r	-	-	-	-	-
He I 6678	-	r	-	-	-	-	-
$v \sin i$ (FT-He)	111 ± 2	67 ± 8	78 ± 4	71 ± 5	73 ± 6	63 ± 11	62 ± 3
$v \sin i$ (FW-He)	137 ± 10	100 ± 11	125 ± 11	105 ± 16	105 ± 21	89 ± 15	90 ± 13
$v \sin i$ (FT-M)	108 ± 4	73 ± 7	66 ± 6	73 ± 4	76 ± 7	55 ± 5	62 ± 6
$v \sin i$ (FW-M)	120 ± 7	95 ± 13	103 ± 10	93 ± 11	94 ± 8	88 ± 7	79 ± 6

Target	CygOB2-2	HD 13854	HD 190603	HD 14956	HD 14143	HD 14818	HD 194279
SpT	B1I	B1Iab	B1.5Ia+	B1.5Ia	B2Ia	B2Ia	B2Ia
Obs. run	WHT03	WHTB	WHTB	WHTB	WHTB	WHTB	WHTB
SNR		250	570	450	450	450	450
C II 4267	43 (50)	54 (78)	49 (54)	(69)	42 (66)	68 (76)	55 (69)
N II 3995		48 (79)	51 (64)	46? (72)	63? (70)	48 (69)	54 (74)
N II 4254	59 (64)	57 (77)	52 (62)	56 (67)	51 (64)	49 (63)	55 (73)
N II 4601	68 (68)	61? (81)	53 (60)	55 (77)	54 (66)	52 (73)	52 (74)
N II 4614		60 (68)	44 (53)	53? (68)	56 (59)	50 (52)	53 (67)
N II 4621		b (73)	49 (54)	52 (69)	52 (67)	50 (68)	52 (66)
N II 4630		52 (84)	52 (63)	54? (76)	53 (73)	54 (70)	59 (74)
Si III 4552	44 (58)	r (85)	50 (68)	55 (76)	48 (70)	47 (74)	49 (75)
Si III 4567	48 (61)	45 (83)	44 (68)	55 (75)	54 (72)	54 (74)	52 (71)
Si III 4574	45 (55)	54 (77)	52 (63)	61 (68)	(66)	60 (68)	52 (68)
Si IV 4089		r (73)	b	d	d	d	d
Si IV 4116	58 (56)	65 (73)	49 (59)	d	d	d	d
O II 4590	42 (67)	r (74)	57 (59)	61 (69)	44 (66)	57 (64)	57 (67)
O II 4595	44 (63)	r (67)	55 (56)	43 (69)	46 (54)	53 (67)	56 (71)
O II 4661	47 (41)	r (76)	52 (58)	48 (69)	47 (59)	54 (68)	48 (67)
He I 4143	b	62(86)	54 (67)	48 (80)	53 (71)	57 (81)	56 (76)
He I 4387	50 (92)	48(90)	46 (74)	48 (87)	53 (81)	61 (85)	59 (82)
He I 4471	b	62(110)	59 (88)	73 (98)	67 (98)	74 (103)	66 (95)
He I 4713	47 (63)	56 (77)	50 (62)	47 (69)	52 (66)	64 (72)	48 (65)
He I 4922	b	-	-	-	-	-	-
He I 5015	49 (67)	-	-	-	-	-	-
He I 5047	49 (58)	-	-	-	-	-	-
He I 5875	59 (82)	-	-	-	-	-	-
He I 6678	50 (79)	-	-	-	-	-	-
$v \sin i$ (FT-He)	51 ± 5	55 ± 7	52 ± 7	48 ± 1	53 ± 1	63 ± 2	54 ± 8
$v \sin i$ (FW-He)	74 ± 13	92 ± 17	75 ± 13	85 ± 15	82 ± 16	87 ± 16	87 ± 15
$v \sin i$ (FT-M)	49 ± 9	55 ± 6	51 ± 4	53 ± 5	51 ± 6	54 ± 6	53 ± 3
$v \sin i$ (FW-M)	58 ± 8	77 ± 6	60 ± 5	71 ± 4	66 ± 6	69 ± 6	71 ± 3

Table 6. Same as Table 3 but for mid-O dwarfs.

Star	HD 12993	CygOB2-16	HD 46056	HD 13268	HD 46966	HD 236894	HD 168137
SpT	O6.5V	O7.5V	O8Vn	ON8V	O8V	O8V	O8.5V
Obs. run	PerOB1	WHT03	CAHA	INT89	INT89	PerOB1	WHT03
SNR							
He I λ 4387	77 (123)	209 (220)	345 (352)	315 (307)	70 (100)	148 (170)	80 (106)
He I λ 4471	80 (90)	214 (230)	350 (404)	310 (320)	54 (98)	142 (176)	59 (110)
He I λ 4713	87 (122)	203 (216)			57 (72)	148 (156)	48 (73)
He I λ 4922	-	191 (217)	359 (371)	298 (301)	54 (80)	-	58 (100)
He I λ 5875	-	201 (224)	-	-		-	53 ()
Si IV λ 4089	84 (90)	b	-	-		144 (152)	53 (79)
Si IV λ 4116	r	b	-	-		b	61 (69)
O III λ 5592	-	213 (238)	-	-	-	-	58 (80)
C IV λ 5801	-	b	-	-	-	-	50 (77)
C IV λ 5811	-	224 (235)	-	-	-	-	50 (77)
$v \sin i$ (FT-He)	81 ± 5	204 ± 9	351 ± 7	308 ± 9	59 ± 8	146 ± 3	61 ± 13
$v \sin i$ (FW-He)	112 ± 9	221 ± 6	376 ± 26	309 ± 10	88 ± 15	167 ± 10	97 ± 17
$v \sin i$ (FT-M)	84	219 ± 8	-	-	-	144	54 ± 5
$v \sin i$ (FW-M)	90	237 ± 2	-	-	-	152	76 ± 4

Table 7. Same as Table 3 but for early and mid-O supergiants. [a] Line in emission.

Star	CygOB2-7	CygOB2-8C	CygOB2-9	CygOB2-11	CygOB2-8A	HD 210839	HD 192639
SpT	O3If	O5If	O5If	O5If+	O5.5I(f)	O6I(n)fp	O7Ib(f)
Obs. run	WHT03	WHT03	WHT03	WHT03	WHT03	INT92	INT89
SNR	250	250	150	200	350	150	220
He I λ 4387	-	-	-	-	-	-	95 (121)
He I λ 4471	-	180 (211)	97 (136)	107 (154)	87 (136)	223 (256)	104 (163)
He I λ 4713	-	-	-	-	84 (102)	-	114 (125)
He I λ 4922	-	-	-	-	-	-	115 (130)
He I λ 5875	94 (117)	170 (205)	97 (119)	120 (134)	82 (125)	-	-
C III λ 5695	-	(249)[a]	104 (120)[a]	120 (140)[a]	98 (118)[a]	-	-
C IV λ 5801	96 (100)[a]	b	b	b	b	-	-
C IV λ 5811	105 (103)[a]	180 (200)	b	117 (143)	84 (120)	-	-
O III λ 5592	-	184 (196)	113 (135)	100 (136)	80 (135)	-	-
Si IV λ 4089	89 (112)[a]	-	-	-	-	-	100 (114)
Si IV λ 4116	89 (112)[a]	(233)[a]	(179)[a]	122 (147)	(108)[a]	-	117 (112)
N III λ 4634	(120)[a]	b	b	b	b	b	b
N III λ 4641	94 (120)[a]	b	b	b	b	b	b
N IV λ 4058	102 (143)	-	-	-	-	-	-
$v \sin i$ (FT-He)	94	175 ± 7	97	114 ± 9	84 ± 3	223	107 ± 9
$v \sin i$ (FW-He)	117	208 ± 4	128 ± 12	144 ± 14	121 ± 17	256	135 ± 19
$v \sin i$ (FT-M)	96 ± 7	182 ± 3	109 ± 6	115 ± 10	87 ± 9		109 ± 12
$v \sin i$ (FW-M)	116 ± 14	220 ± 26	145 ± 31	142 ± 5	120 ± 11		113 ± 1

Table 8. Same as Table 3 but for OB giants with $v \sin i$ values below 100 km s^{-1}.

Star	CygOB2-8B	CygOB2-4	HD 164492A	HD 168504
SpT	O6.5III	O7III(f)	O7.5III	O8III
Obs. run	WHT03	WHT03	INT02	WHT03
SNR	230	220	250	300
He I λ4387	d	d	45 (89)	88 (112)
He I λ4471	74 (130)	83 (120)	49 (94)	79 (129)
He I λ4713		82 (118)	52 (61)	77 (90)
He I λ4922	-	(128)	52 (80)	
He I λ5015	94 (115)	85 (116)	48 (60)	
He I λ5875	85 (115)	80 (130)		
C IV λ5811	83 (110)	70 (136)	-	
N II λ4254	65 (118)	74 (125)		
O III λ5592	82 (118)	74 (125)	-	
Si IV λ4089	84 (119)	84 (125)	50 (61)	
Si IV λ4116		81 (103)	45 (56)	85 (89)
Si IV λ4212			50 (51)	81 (81)
Si IV λ4654			45 (51)	76 (81)
$v \sin i$ (FT-He)	84 ± 10	83 ± 2	49 ± 3	81 ± 6
$v \sin i$ (FW-He)	120 ± 9	122 ± 6	77 ± 16	110 ± 20
$v \sin i$ (FT-M)	79 ± 9	77 ± 6	48 ± 3	81 ± 5
$v \sin i$ (FW-M)	116 ± 4	123 ± 12	55 ± 5	84 ± 5

Table 9. Same as Table 3 but for OB giants with high $v \sin i$.

Star	HD 24912	HD 203064	HD 191423
SpT	O7III(n)((f))	O7.5III:n((f))	O9III:n
Obs. run	INT89	INT89	INT89
SNR	250	200	
He I λ4387	224 (247)		
He I λ4471	211 (247)	317 (338)	468 (470)
He I λ4713	225 (242)	330 (322)	
He I λ4922	215 (230)	328 (335)	429 (437)
$v \sin i$ (FT-He)	219 ± 7	325 ± 7	450 ± 30
$v \sin i$ (FW-He)	242 ± 8	332 ± 9	454 ± 23

Table 10. Summary of $v \sin i$ values derived for the sample of studied stars. All $v \sin i$ values correspond to metal lines measurements except those marked with $^{(a)}$, where He I were used. See text for references on effective temperature and luminosity determinations.

Star	SpT	$v \sin i$(FT)	$v \sin i$(FWHM)	$T_{\rm eff}$(K)	$\log L/L_{\odot}$	Ref
CygOB2-7	O3If*	96 ± 7	116 ± 14	45 500	5.91	He02
CygOB2-8C	O5I(f)	182 ± 3	220 ± 26	41 000	5.66	He02
CygOB2-9	O5If+	109 ± 6	145 ± 31	38 610	5.87	Mar05
CygOB2-11	O5I(f)+	115 ± 10	142 ± 5	37 000	5.92	He02
CygOB2-8A	O5.5If	87 ± 9	124 ± 9	38 500	6.19	He02
HD 210839	O6I(n)fp	$223^{(a)}$	$256^{(a)}$	36 000	5.83	Rep04
HD 192639	O7Ib(f)	109 ± 12	113 ± 1	35 000	5.68	Rep04
HD 210809	O9Iab	108 ± 4	120 ± 7	31 500	5.60	Rep04
CygOB2-10	O9.5Iab	71 ± 9	95 ± 12	29 000	5.77	He02
HD 209975	O9.5Iab	66 ± 6	103 ± 10	32 000	5.69	Rep04
HD 167264	B0Ia	73 ± 4	93 ± 11	29 558	5.53	Mar05
HD 37128	B0Ia	76 ± 7	94 ± 8	27 500	5.69	Urb04
HD 38771	B0.5Ia	55 ± 5	88 ± 7	26 500	4.94	Urb04
HD 2905	BC0.7Ia	62 ± 6	79 ± 6	21 500	5.52	Cro06
CygOB2-2	B1I	49 ± 9	58 ± 8	28 000	4.85	He02
HD 13854	B1Iab	55 ± 6	77 ± 6	21 700	5.92	Urb04
HD 190603	B1.5Ia+	51 ± 4	60 ± 5	18 500	5.57	Cro06
HD 14956	B1.5Ia	53 ± 5	71 ± 4	20 500	5.66	Urb04
HD 14143	B2Ia	51 ± 6	66 ± 6	19 500	5.48	Urb04
HD 14818	B2Ia	54 ± 6	69 ± 6	20 100	5.47	Urb04
HD 194279	B2Ia	53 ± 3	71 ± 3	19 000	5.37	Cro06
CygOB2-8B	O6.5III(f)	79 ± 9	116 ± 4	37 130	5.54	Mar05
HD 24912	O7III(n)((f))	$219 \pm 7^{(a)}$	$242 \pm 8^{(a)}$	35 000	5.42	Rep04
CygOB2-4	O7III(f)	77 ± 6	123 ± 12	35 500	5.41	He02
HD 164492A	O7.5III	48 ± 3	55 ± 5	35 020	5.42	Mar05
HD 203064	O7.5III:n((f))	$325 \pm 7^{(a)}$	$332 \pm 9^{(a)}$	34 500	5.50	Rep04
HD 168504	O8III	81 ± 5	84 ± 5	33 960	5.35	Mar05
HD 191423	O9III:n	$450 \pm 30^{(a)}$	$454 \pm 23^{(a)}$	32 500	5.23	Rep04
HD 12993	O6.5V	84	90	37 870	5.23	Mar05
CygOB2-16	O7.5V	219 ± 8	237 ± 2	35 870	5.05	Mar05
HD 46056	O8V((f))	$351 \pm 7^{(a)}$	$380 \pm 30^{(a)}$	34 980	4.96	Mar05
HD 13268	ON8V	$308 \pm 9^{(a)}$	$309 \pm 10^{(a)}$	33 000	5.05	Rep04
HD 46966	O8V	$59 \pm 8^{(a)}$	$88 \pm 14^{(a)}$	34 880	4.96	Mar05
HD 236894	O8V	144	152	34 880	4.96	Mar05
HD 168137	O8.5V	54 ± 5	76 ± 4	33 879	4.86	Mar05
HD 37041	O9V	$132 \pm 5^{(a)}$	165 ± 21	35 000	4.93	SD06
HD 214680	O9V	37 ± 3	43 ± 4	36 000	5.02	SD06
HD 149757	O9V	$390 \pm 17^{(a)}$	$414 \pm 18^{(a)}$	32 880	4.77	Mar05
BD-134928	O9.5Vn	$410 \pm 13^{(a)}$	$420 \pm 8^{(a)}$	31 880	4.68	Mar05
CygOB2-23	O9.5V	$162 \pm 8^{(a)}$	$177 \pm 20^{(a)}$	31 880	4.68	Mar05
CygOB2-145	O9.5V	38 ± 4	28 ± 8	31 880	4.68	Mar05
τ Sco	B0.2V	≤ 13	14 ± 3	32 000	4.47	SD06
HD 37020	B0.5V	53 ± 3	54 ± 3	30 000	4.45	SD06
HD 37023	B0.5V	50 ± 3	60 ± 8	32 000	4.47	SD06
HD 37042	B0.5V	34 ± 3	36 ± 4	29 000	4.11	SD06
HD 217657	B0.5V	34 ± 5	31 ± 6	29 888	4.50	Mar05
HD 228199	B0.5V	112 ± 8	121 ± 6	29 888	4.50	Mar05
HD 37061	B1V	$217 \pm 3^{(a)}$	$231 \pm 23^{(a)}$	32 000	4.54	SD05
ω^1 Sco	B1V	101 ± 4	105 ± 5	28 890	4.41	Mar05